Author/s:
Russell, BJ;Cadusch, JJ;Meng, J;Wen, D;Crozier, KB

Title:
Mid-infrared spectral reconstruction with dielectric metasurfaces and dictionary learning

Date:
2022-05-15

Citation:
Russell, B. J., Cadusch, J. J., Meng, J., Wen, D. & Crozier, K. B. (2022). Mid-infrared spectral reconstruction with dielectric metasurfaces and dictionary learning. Optics Letters, 47 (10), pp.2490-2493. https://doi.org/10.1364/OL.448858.

Mid-Infrared Spectral Reconstruction with Dielectric Metasurfaces and Dictionary Learning

Benjamin Russell,[1,2] Jasper J. Cadusch,[2,3] Jiajun Meng,[1,2,3] Dandan Wen,[3,4] and Kenneth B. Crozier[1,2,3,*]

[1]*School of Physics, University of Melbourne, Victoria 3010, Australia*
[2]*Australian Research Council (ARC) Centre of Excellence for Transformative Meta-Optical Systems (TMOS)*
[3]*Department of Electrical and Electronic Engineering, University of Melbourne, Victoria 3010, Australia*
[4]*Shaanxi Key Laboratory of Optical Information Technology, School of Physical Science and Technology, Northwestern Polytechnical University, Xi'an 710124, China*
*kcrozier@unimelb.edu.au

Abstract: Mid-infrared (MIR) spectroscopy has numerous industrial applications and is usually performed with Fourier transform infrared (FTIR) spectrometers. While these work well for many purposes, there is currently much interest in alternative approaches that are smaller and lighter, i.e. MIR microspectrometers. Here we investigate all-dielectric metasurfaces as spectral filters for MIR microspectrometers. Two metasurface types are studied. For the first, we design, fabricate, and test a metasurface with a narrow and angularly tunable transmission stopband. We use it to reconstruct the transmission spectra of various materials. The second metasurface, investigated theoretically, possesses narrow passband features via symmetry-protected bound states in the continuum.

1. Introduction

Mid-infrared (MIR) spectroscopy is well-suited to the non-destructive analysis of many chemicals such as alcohols, amines, and aromatic solvents. While numerous microspectrometers have been demonstrated at visible and near-infrared wavelengths, notably fewer have been created for the MIR [1-8]. An established microspectrometer design involves the integration of a spectral filter array with an array of photodetectors. These are often referred to as filter array - detector array (FADA) spectrometers. The filter transmission spectra and the photocurrents produced by each filter-detector pair in the presence of an unknown spectrum are fed to a reconstruction algorithm to determine the spectrum. Plasmonic metasurfaces have proven to be effective spectral filters in FADA and MEMS microspectrometers [3-6]. However, the quality of their filter functions are inevitably limited by loss. This motivates the development of spectral filters for MIR spectroscopy that achieve low loss and sharper filter functions using dielectric materials, i.e. dielectric metasurfaces. These filters have recently been the topic of much interest in the MIR, e.g., for the spectral fingerprinting of locally adsorbed molecules [9]. Dielectric metasurfaces can also have the added benefit of angularly tunable transmission spectra, suggesting that one could realize an MIR microspectrometer by combining a single angularly tunable metasurface with a photodetector (rather than an array of both filters and detectors) [10]. In this work, we study a dielectric metasurface suited to this approach (i.e. single metasurface and angular tuning) and a FADA configuration, and consider both bandstop and bandpass designs. The organization of this Letter is as follows. We first describe the design, fabrication, and testing of a dielectric metasurface that functions as a

bandstop filter. We furthermore demonstrate its use for the spectral reconstruction of various materials using a dictionary learning algorithm. We next explore the design of a metasurface that functions as a bandpass filter. Our paper concludes with a discussion of future applications.

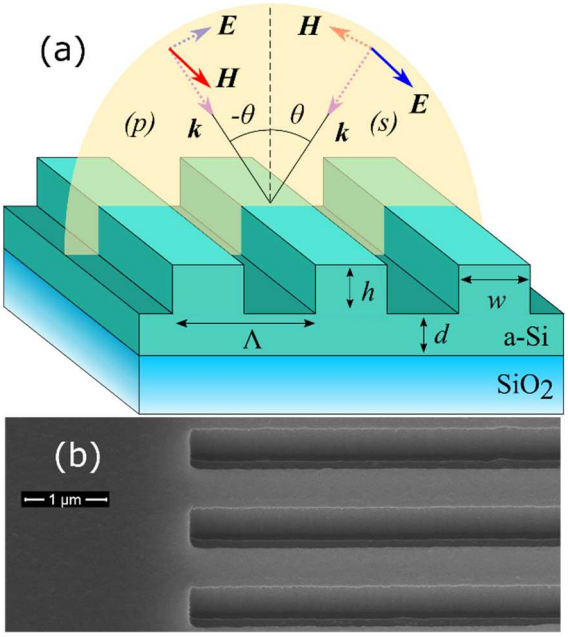

Fig 1. (a) Schematic illustration of the dielectric metasurface studied in this work. Diagram shows definitions of metasurface geometry (Λ, d, w, h), angle (θ), the plane of incidence, and the field components of *s* and *p* polarized incident rays. (b) Scanning electron micrograph image of a test metasurface used to validate fabrication methods, Λ = 1100nm, d = 410nm, w/Λ = 0.5, and h = 760nm, imaged at an angle of 30 degrees from the zenith.

The metasurfaces we study in this paper are a subset of guided mode resonance filters dubbed zero-contrast gratings (ZCGs) due to the presence of a grating layer (thickness *h*) on a waveguide layer (thickness *d*) with identical refractive index (Fig. 1a) [11-13]. Our metasurface was inspired by investigations into angularly tunable stopbands in transmission within a transparent background [12]. We fabricated an amorphous silicon metasurface on glass (Fig. 1a) using geometric parameters optimized for strong reflection resonances in the 1.5 - 3.5 μm waveband. These parameters were as follows: Λ = 950nm, d = 373nm, w/Λ = 0.643, and h = 132nm. The overall extent of our ZCG was 5 mm × 10 mm. Fabrication began with plasma enhanced chemical vapor deposition of a silicon film (505 nm thick), followed by e-beam lithography to expose a grating etch mask, and reactive ion etching to produce the grating trenches. A scanning electron micrograph of a test metasurface confirmed smooth and vertical sidewalls (Fig. 1b).

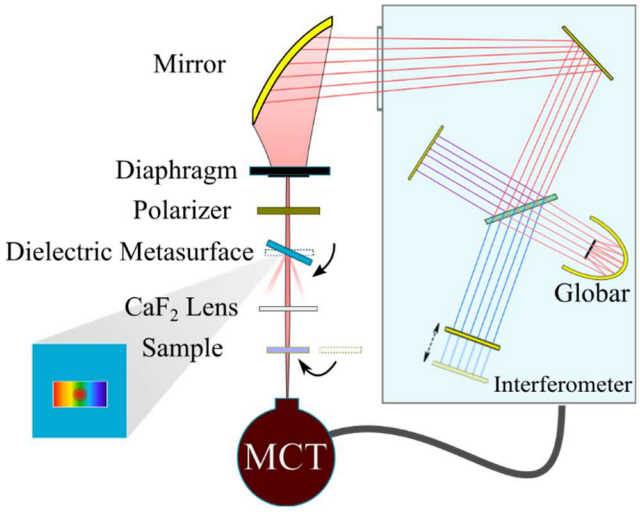

Fig 2. Setup used for characterization of dielectric metasurface and for the reconstruction of transmission spectra of various samples. Inset: schematic illustration, showing approximate size of beam (~2.5 mm diameter) on metasurface (5mm×10mm) at normal incidence.

The set-up we used to characterize the fabricated metasurface is illustrated schematically in Fig. 2. Infrared light emerging from the external port of a Fourier-transform infrared spectrometer (FTIR, Perkin Elmer Frontier) was polarized by a wire grid polarizer and illuminated the patterned side of the metasurface, which was mounted on a manual rotation stage. A variable aperture was employed to restrict the spot size and angular distribution of the incident beam at the metasurface plane. The light transmitted through the metasurface was focused by a calcium fluoride (CaF_2) lens onto a mercury cadmium telluride (MCT) photodetector, whose amplified output was fed to the external detector input of the FTIR system. Experimental results obtained with this set-up are shown in Fig. 3 alongside simulation.

Finite element method (FEM) simulations of a single grating under periodic (Floquet) boundary conditions were performed in COMSOL Multiphysics' wave optics module with the smallest available geometry mesh preset (extremely fine) to ensure convergence. These simulations calculated the metasurface transmission T_{meta} for light incident from the air and exiting into the glass substrate. To bypass complete FEM simulation of the 750 μm thick substrate, we modelled it as an incoherent, plane-parallel optical cavity with mirror reflectivities dictated by the Fresnel equations.

$$T_{\text{substrate}} = T_1 e^{-\alpha q(\theta)} / 1 - R_1 R_2 e^{-2\alpha q(\theta)} \quad (1)$$

The T_n and R_n are the polarization-specific Fresnel (power) coefficients, with subscripts 1 and 2 denoting glass-to-air and glass-to-silicon interfaces, respectively. The loss coefficient α was determined from normal incidence measurements of an unpatterned glass substrate, and an effective cavity length $q(\theta)$ was derived using Snell's law to trace ray lengths within the substrate. The metasurface's transmission spectrum was given as the product of this substrate transmission and T_{meta}. These simulations (Fig. 3) were in very good agreement with our measurement, with any remaining discrepancies attributable to imperfections in metasurface fabrication, beam collimation, and the substrate transmission model. The transmission spectra of our metasurfaces displayed strong variation with the angle of incidence (Fig. 3). We could therefore realize a microspectrometer that utilizes the metasurface as the sole filtering element by mounting it on a rotation stage and using a single photodetector to measure transmitted power at multiple angles. An algorithm could then be used to reconstruct the spectrum from this data.

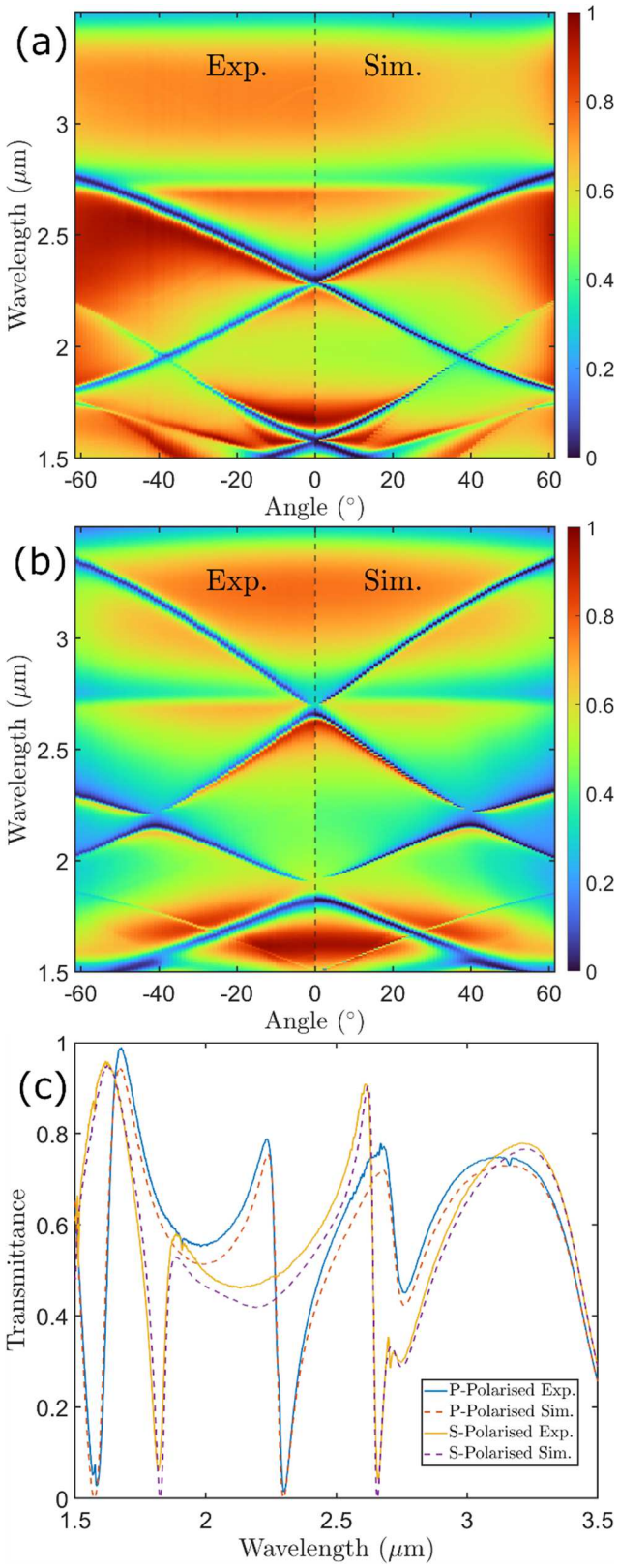
(a)
Exp.
Sim.
Wavelength (μm)
Angle (°)
(b)
Exp.
Sim.
Wavelength (μm)
Angle (°)
(c)
Transmittance
Wavelength (μm)
P-Polarised Exp.
P-Polarised Sim.
S-Polarised Exp.
S-Polarised Sim.

Fig 3. Heatmaps of the ZCG's transmission for (a) *p* and (b) *s* incidence. $\theta < 0$ regions represent simulated transmission ("Sim") while $\theta > 0$ regions represent FTIR measurements ("Exp"). The simulations consider losses from Fresnel reflections and absorption within the substrate. (c) Simulated & measured transmission at normal incidence.

To demonstrate this concept, we reappropriated the characterization setup (Fig. 2). To mimic the signal that would be recorded by the photodetector in a microspectrometer, we integrated the spectrum measured by our FTIR-based system over the spectral band of operation at each metasurface angle for both polarizations. The use of both polarizations improves the spectral reconstruction as they have distinct transmission spectra (Fig. 3). A reconstructed spectral power distribution (SPD) was then recovered using a two-part algorithm. The first part was based on recursive least squares (RLS) filtering which provides solutions to ill-posed systems of equations of the form

$$\mathbf{y} = \mathbf{A} \cdot \mathbf{x} + \varepsilon \tag{2}$$

Such that the error (ε) is minimized. The detector, receiving light filtered by the metasurface at M discrete angles produced an M×1 photocurrent vector $\mathbf{y}$. This was represented by the integral over wavelength of the product of the metasurface transmission, the SPD, and detector responsivity. The transmission spectrum of the metasurface, recorded at these same angles at a spectral resolution of N points populated an M×N matrix $\mathbf{A}$. Here we have M=122, because spectra are measured from 0° to 60° (steps of 1°) and the two polarisations are combined to give $\mathbf{A}$. This means that $\mathbf{x}$ is an $N \times 1$ vector that represented the product of the detector responsivity and the unknown SPD of the light source. In the first part of the algorithm, we used a dictionary learning algorithm to transform the reconstruction problem to a vector space that facilitates sparse representations of the SPD. The second part of our algorithm used the standard RLS method to solve for the transformed SPD. For the DLA, we used a set of deidentified spectra to train an N×K transformation matrix $\mathbf{D}$ with columns dubbed 'atoms' [14-17]. This matrix minimizes error when training spectra are encoded as sparse and linear combinations of the atoms. We used this matrix solve for the sparse, K×1 coefficient vector ($\mathbf{s}$) that can be transformed back to wavelength-space vector $\mathbf{x}$.

$$\mathbf{x} = \mathbf{D} \cdot \mathbf{s} \tag{3.1}$$

$$\mathbf{y} = \mathbf{A} \cdot \mathbf{D} \cdot \mathbf{s} \underset{\mathbf{RLS}}{\longrightarrow} \mathbf{min}|\mathbf{y} - \mathbf{A} \cdot \mathbf{D} \cdot \mathbf{s}|^2 \tag{3.2}$$

First, we reconstructed the spectrum produced by our FTIR system's incoherent, broadband, IR thermal radiation source, a silicon carbide rod (globar) identical to that of refs. [3,4], without attenuation (Fig. 4a). The discrepancy between reconstruction result $\mathbf{x}$ and the SPD measured directly by the FTIR $\mathbf{x'}$ was quantified via a normalized root-mean-square deviation (NRMSD) calculation.

$$\text{NRMSD} = \sqrt{\frac{1}{N}\sum_n^N \frac{(\mathbf{x'}_n - \mathbf{x}_n)^2}{(\mathbf{x'}_{\max} - \mathbf{x'}_{\min})^2}} \tag{4}$$

Subsequent results shown in Fig. 4b–d depict the attenuation of the globar spectrum by a set of MIR transparent materials: a neutral density filter, polymethyl methacrylate (PMMA), and an acetone-filled fluid cell. It can be seen that all results were in reasonable agreement with the FTIR measurements. The latter were taken with linearly-polarized light.

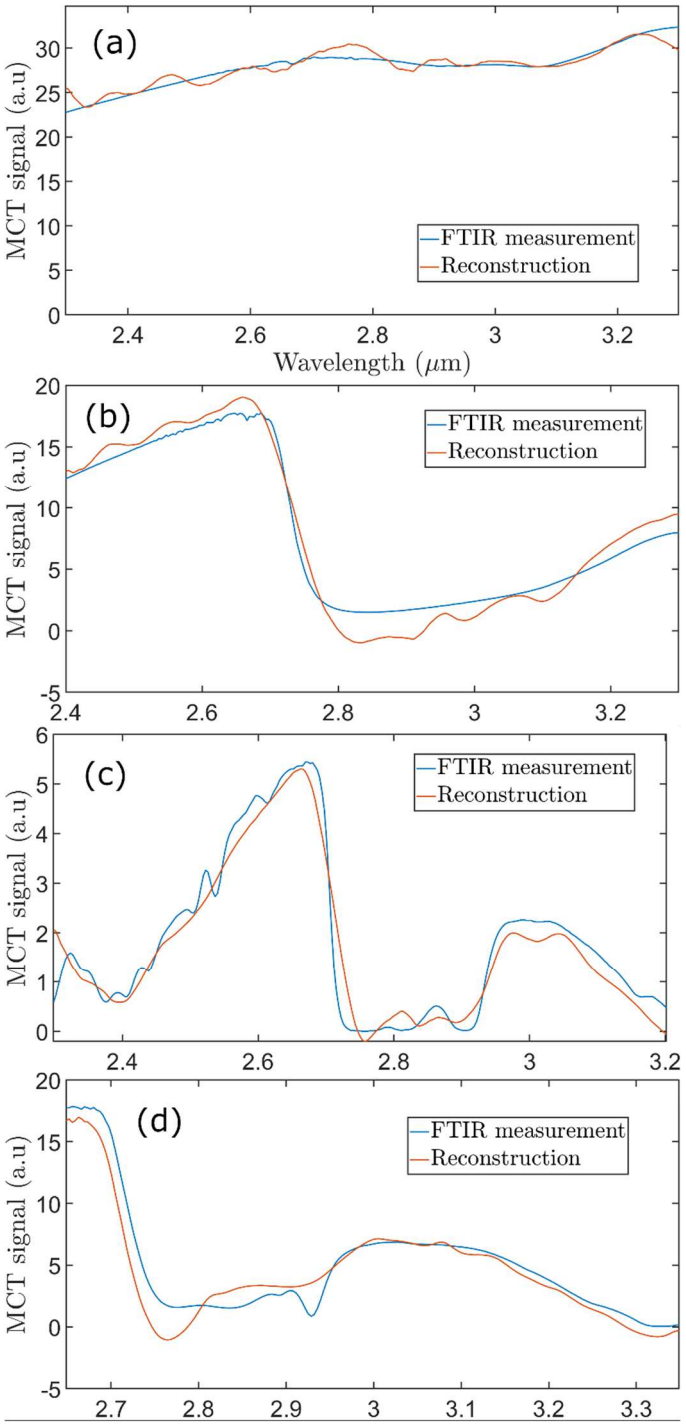

Fig 4. Reconstructions of the globar SPD attenuated by various materials. (a) No attenuation, NRMSD = 0.0787. (b) a neutral density filter, NRMSD = 0.0751. (c) a 0.79mm thick PMMA window, NRMSD = 0.0698. (d) an acetone fluid cell constructed from two 1mm thick microscope slides and a 127μm thick parafilm gasket, NRMSD = 0.0774.

The metasurface described thus far can be termed a bandstop filter. Below, we discuss modifying the grating geometry to achieve bandpass functionality. Our design process started by adapting the ZCG discussed in Ref [18] to the MIR for a different transparent substrate (CaF_2). In Ref [18], the aim is broad reflection bands. Here, we instead focused on generating narrowband resonances in transmission. We simulated asymmetric transmission resonances within this band using obliquely incident light. These resonances result from an interference phenomenon known as the bound state in the continuum (BIC) [19-20]. In this ZCG, symmetry-protected BICs emerge within the waveguide layer from the destructive interference of counterpropagating diffracted modes of matched order. Perturbation to the symmetry of the propagation plane compromises the bound state, producing a high-Q, Quasi-BIC feature with a finite linewidth correlated with the magnitude of the perturbation [20]. This concept can be used to realize arrays of filters with distinct, linewidth-tunable transmission resonances by scaling each dimension of the filter geometry linearly (Fig. 5). By integrating these filters with an array of detectors, spectral datapoints could be read directly from the photocurrents avoiding algorithmic reconstruction [10].

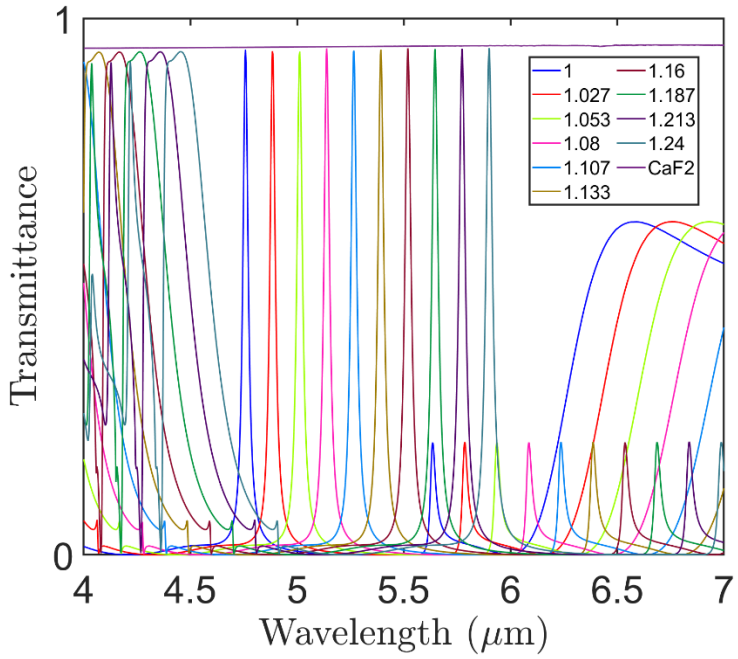

Fig 5. Simulated transmission for a set of quasi-BIC filters based on a metasurface with Λ = 2364nm, d = 774nm, w/Λ = 0.642, h = 1378nm on a 1mm thick CaF_2 substrate. The entire metasurface geometry was multiplied by scale factors ranging from 1 to 1.24 (see figure legend). The angle of incidence was fixed at 4 degrees. Principal resonances span the 4.75-6 µm waveband.

A set of M distinct filters of this type would require the production of as many silicon films, each with a different thickness. However, prior work on Fabry-Perot filter arrays has shown that this can be accomplished in $log_2(M)$ steps using a set of mutually orthogonal, binary masks for deposition and etching [21]. Alternatively, wedge-shaped films, with a tapered thickness have been produced through photoresist reflow and masked lithography [22-23]. These could facilitate fabrication of many-element filter arrays with a single deposition step

Conclusion

We demonstrated a microspectrometer concept that exploits the zeroth order transmission of a dielectric-grating metasurface and the angular tunability of its transmission resonances to computationally reconstruct the transmission spectra of MIR-transparent materials. Transmission spectra of our fabricated

metasurface were in very agreement with simulations. We demonstrated this microspectrometer concept by using the metasurface to measure the transmission spectra of a variety of samples. The results were found to be in good agreement with transmission spectra measured using an FTIR. We furthermore discussed an alternate metasurface design that possessesd tunable-width bandpass resonances that could be used for direct-readout microspectrometers.

Funding

This work was supported in part by the Australian Research Council (ARC) Centre of Excellence for Transformative Meta-Optical Systems (Project ID CE200100010).

Acknowledgements

This work was performed in part at the Melbourne Centre for Nanofabrication (MCN) in the Victorian Node of the Australian National Fabrication Facility (ANFF). We thank Dr James Bullock and Dr Sivacarendran Balendhran for discussions regarding experiment design.

Disclosures

The authors declare no conflicts of interest.

Data Availability

Underlying data is not publicly available but can be obtained from the authors upon reasonable request.

References

1. R. F. Wolffenbuttel, IEEE Trans. Instrum. Meas. 53(1), 197-202, (2004).
2. J. Bao and M. G. Bawendi, Nature, 523, 7558, pp 6770, (2015).
3. B. J. Craig, V. R Shrestha, J. Meng, J. J. Cadusch, K. B. Crozier, Opt. Lett. 43(18), 4481, (2018).
4. B. J. Craig, J. Meng, V. R. Shrestha, J. J. Cadusch, K. B. Crozier Sci. Rep. 9, 13537, (2019).
5. A. Wang, Y. Dan, Sci. Rep. 8, 11257, (2018).
6. T. Stark, M. Imboden, S. Kaya, A. Mertini, J. Chang, S. Erramilli, D. Bishop, ACS Phot. 3(1) pp. 14-1 (2016)
7. A. Tittl, A . Leitis, M. Lui, F. Yesilkoy, D. Choi, D. N. Neshev, Y. S. Kivshar, H. Altug, Science, 360, 1105-1109, 6393 (2018).
8. R. Bhargava, App. Spectroscopy, 66(10), 1091-1120, (2012).
9. F. Yesilkoy, E. R. Arvelo, Y. Jahani, M. Liu, A. Tittl, V. Cevher, H. Altug, Nat. Photonics, 13(6), 390-396, (2019).
10. A. Leitis, A. Tittl, M. Liu, B. H. Lee, M. B. Gu, Y. S. Kivshar, H. Altug, Sci. Adv. 5(5), 1-9, (2019).
11. M. Shokooh-Saremi and R. Magnusson, Opt. Lett. 39(24), 6958, (2014).
12. Y. Zhong, Z. Goldenfield, K. Li, W. Streyer, .L. Yu, L. Nordin, N. Murphy, D. Wasserman, Opt. Lett. 42(2), 223, (2017).
13. R. Magnusson and S. S. Wang, App. Phys. Lett. 61(9), pp. 1022-1024, (1992).
14. K. Skretting and K. Engan, IEEE Trans. Signal Process. 58(4), 2121-2130, (2010).
15. K. Skretting, Dictionary learning tools for MATLAB, University of Stavanger, https://www.ux.uis.no/~karlsk/dle/
16. S. Zhang, Y. Dong, H. Fu, S. Huang, L. Zhang, Sensors (Basel), 18(2), (2018).
17. U. Ultzinger, Spectral Database hosted at the University of Arizona, Available: http://spectra.arizona.edu/.
18. R. Magnusson, Opt. Lett. 39(15), 4337, (2014).
19. C. W. Hsu, B. Zhen, A. D. Stone, J. D. Joanopoulos, M. Soljačić, Nat. Rev. Mat. 1(9), (2016).
20. K. Koshelev, S. Lepeshov, M. Liu, A. Bogdanov, Y. Kivshar, Phys. Rev. Lett. 121(19), (2018).
21. E. Huang, Q. Ma, Z. Liu, Sci. Rep. 7, 40693 (2017).
22. A. Emadi, H. Wu, S. Grabarnik. G. De Graaf, K. Hedsten, P. Enoksson, J.H. Correia, R. F. Wolffenbuttel Sens. Actuators A, 162, pp. 400-405, (2010).
23. J. Loomis, J Micro Nanolithogr MEMS MOEMS, 15(1), (2016).

Uncondensed reference list

1. R. F. Wolffenbuttel, "State-of-the-art in integrated optical microspectrometers", *IEEE Transactions on Instrumentation and Measurement*. **53**(1), 197-202, (2004).
2. J. Bao and M. G. Bawendi, "A colloidal quantum dot spectrometer", *Nature*, **523**, 7558, pp 6770, (2015).
3. B. J. Craig, "Experimental demonstration of infrared spectral reconstruction using plasmonic metasurfaces", *Optics Letters,* **43**(18), 4481, (2018).
4. B. J. Craig, "Mid- to long-wave infrared computational spectroscopy using a subwavelength coaxial aperture array", *Scientific Reports,* **9**(1), 1-11, (2019).
5. A. Wang, Y. Dan, "Mid-infrared plasmonic multispectral filters", *Scientific Reports*, **8**, 11257, (2018).
6. T. Stark, M. Imboden, S. Kaya, A. Mertini, J. Chang, S. Erramilli, D. Bishop, "MEMS tunable Mid-infrared Plasmonic Spectrometer", *ACS Photonics*. **3**(1) pp. 14-19 (2016).
7. A. Tittl, "Imaging-based molecular barcoding with pixelated dielectric metasurfaces", *Science*, **360**, 1105-1109, 6393 (2018).
8. R. Bhargava, "Infrared Spectroscopic Imaging: The Next Generation" *Applied Spectroscopy*, **66**(10), 1091-1120, (2012)
9. F. Yesilkoy, "Ultrasensitive hyperspectral imaging and biodetection enabled by dielectric metasurfaces", *Nature Photonics*, **13**(6), 390-396, (2019).
10. A. Leitis, "Angle-multiplexed all-dielectric metasurfaces for broadband molecular fingerprint retrieval", *Science Advances,* **5**(5), 1-9, (2019).
11. M. Shokooh-Saremi and R. Magnusson, "Properties of two-dimensional resonant reflectors with zero-contrast gratings", *Optics Letters.* **39**(24), 6958, (2014).
12. Y. Zhong, "Mid-wave infrared narrow bandwidth guided mode resonance notch filter", *Optics Letters* **42**(2), 223, (2017).
13. R. Magnusson and S. S. Wang, "New principle for optical filters", *Applied Physics Letters* **61**(9), pp. 1022-1024, (1992).
14. K. Skretting and K. Engan, "Recursive least squares dictionary learning algorithm", *IEEE Transactions on Signal Processing,* **58**(4), 2121-2130, (2010).
15. K. Skretting, "*Dictionary learning tools for MATLAB"*, University of Stavanger, https://www.ux.uis.no/~karlsk/dle/
16. S. Zhang, "A spectral reconstruction algorithm of miniature spectrometer based on sparse optimization and dictionary learning", *Sensors (Basel)*, **18**(2), (2018).
17. U. Ultzinger, "*Spectra Database hosted at the University of Arizona.*" Available: http://spectra.arizona.edu/.
18. R. Magnusson, "Wideband reflectors with zero-contrast gratings", *Optics Letters,* **39**(15), 4337, (2014).
19. C. W. Hsu, "Bound states in the continuum", *Nature Review Materials,* **1**(9), (2016).
20. K. Koshelev, "Asymmetric Metasurfaces with High- Q Resonances Governed by Bound States in the Continuum", *Physical Review Letters,* **121**(19), (2018).
21. E. Huang, "Etalon Array Reconstructive Spectrometry", *Scientific Reports,* **7**, 40693 (2017).
22. A. Emadi, "Fabrication and characterization of IC-Compatible Linear Variable Optical Filters with application in a micro-spectrometer", *Sensors and Actuators* A, **162**, pp. 400-405, (2010).
23. J. Loomis, "Grayscale Lithography – Automated mask generation for complex three-dimensional topography" *Journal of Micro/Nanolithography, MEMS, and MOEMS*, **15**(1), (2016).